Attosecond Control in Photoionization of Hydrogen Molecules

F. Kelkensberg,[1] W. Siu,[1] J. F. Pérez-Torres,[2] F. Morales,[2,3] G. Gademann,[1] A. Rouzée,[1,3] P. Johnsson,[1,4] M. Lucchini,[5] F. Calegari,[5] J. L. Sanz-Vicario,[6] F. Martín,[2,7] and M. J. J. Vrakking[1,3]

[1]*FOM Institute AMOLF, Science Park 104, 1098 XG Amsterdam, The Netherlands*
[2]*Departamento de Química, Módulo 13, Universidad Autónoma de Madrid, 28049 Madrid, Spain*
[3]*Max-Born-Institut, Max-Born Strasse 2A, D-12489 Berlin, Germany*
[4]*Department of Physics, Lund University, PO Box 118, SE-221 00 Lund, Sweden*
[5]*Department of Physics, Politecnico di Milano, Istituto di Fotonica e Nanotecnologie CNR-IFN, Piazza Leonardo da Vinci 32, 20133 Milano, Italy*
[6]*Grupo de Física Atómica y Molecular, Instituto de Física, Universidad de Antioquia, AA1226 Medellín, Colombia*
[7]*Instituto Madrileño de Estudios Avanzados en Nanociencia (IMDEA-Nanociencia), Cantoblanco, 28049 Madrid, Spain*

(Received 19 January 2011; published 19 July 2011)

We report experiments where hydrogen molecules were dissociatively ionized by an attosecond pulse train in the presence of a near-infrared field. Fragment ion yields from distinguishable ionization channels oscillate with a period that is half the optical cycle of the IR field. For molecules aligned parallel to the laser polarization axis, the oscillations are reproduced in two-electron quantum simulations, and can be explained in terms of an interference between ionization pathways that involve different harmonic orders and a laser-induced coupling between the $1s\sigma_g$ and $2p\sigma_u$ states of the molecular ion. This leads to a situation where the ionization probability is sensitive to the instantaneous polarization of the molecule by the IR electric field and demonstrates that we have probed the IR-induced electron dynamics with attosecond pulses.

DOI: 10.1103/PhysRevLett.107.043002 PACS numbers: 33.80.Eh, 42.65.Ky, 82.53.Eb

The prospect of observing and controlling ultrafast electron dynamics in molecular systems is the basis of the current interest to apply attosecond (1 as $= 10^{-18}$ s) laser pulses to physical chemistry. Since the first demonstration of attosecond pulses [1,2], pioneering experiments have demonstrated their potential in atoms [3,4], solid state systems [5], and, most recently, molecules [6], where interest has been stimulated by numerical studies which suggest that an electronic (i.e., attosecond or few-femtosecond) time scale may be important in fundamental chemical processes [7,8]. The inherent multielectron nature of the electron dynamics in many molecular systems is a formidable challenge to theoreticians and experimentalists alike, and requires the development of novel theoretical and experimental techniques.

Attosecond pump-probe spectroscopy is based on the generation of attosecond light pulses by high harmonic generation. Presently, attosecond pulses exist as attosecond pulse trains (APTs) [1] and as isolated attosecond pulses [2]. The first application of attosecond pulses to follow rapid electron dynamics in a molecule revealed that the dissociative ionization of hydrogen by a two-color extreme-ultraviolet (XUV) + IR field results in a localization of the bound electron in the molecular ion that depends with attosecond time resolution on the time delay between the attosecond XUV pulse and the IR laser pulse [6]. This could be observed via an asymmetry of the ejected fragments in the laboratory frame, i.e., after the dissociation was complete [9]. A similar experimental result was also obtained using an APT [10]. In these experiments the attosecond pulses initiated electron dynamics that was subsequently addressed by an IR pulse. A next challenge is to use attosecond pulses as a probe of ultrafast molecular electron dynamics. In this Letter we do so by investigating how a moderately intense IR field influences the electronic states that are accessed in photoionization of hydrogen using an APT.

In the experiment, an XUV APT (with two pulses per IR cycle) and a 30 fs FWHM 780 nm (IR) pulse (3×10^{13} W/cm^2) with identical linear polarization were collinearly propagated and focused onto an ensemble of hydrogen or deuterium molecules. High harmonic generation in krypton created odd harmonics H11 up to H27. Such a spectrum allows direct ionization to the first excited ionic state ($2p\sigma_u$), but limits the excitation of higher-lying states as much as possible. The three-dimensional velocity distributions of H^+ and D^+ were measured using a velocity map imaging spectrometer [11] with a gas-injection system integrated into the repeller electrode [12]. The delay between the APT and the IR field was scanned in steps of 200 as, i.e., at an approximately 10 times higher time resolution than in Ref. [13], where vibrational wave packet dynamics was investigated. Although only results for deuterium molecules will be presented here, hydrogen molecules show analogous behavior.

In Figs. 1(a) and 1(b) fragment kinetic energy spectra resulting from the interaction of D_2 with the APT only are shown for fragments ejected parallel and perpendicular to

the laser polarization (black solid lines). We choose to present the measurements in this form (rather than in the form of a total fragment kinetic energy spectrum and an angular distribution), since at different angles different ionic states play a role. For these angle-specific spectra, here and in the remainder of this Letter, an acceptance angle of $\pm 20°$ was used. Figure 1(c) shows a D^+ momentum map resulting from dissociative ionization by the APT. Several contributions can be distinguished that can be related to Fig. 1(d), where a potential energy diagram representing the relevant states is given. Direct ionization to the $1s\sigma_g$ ground state primarily produces stable D_2^+, with a small dissociative part ($\sim 2\%$) that results in a low kinetic energy peak ($E_k < 1$ eV) in Figs. 1(a) and 1(b). The main contribution between 1 and 5 eV, which peaks along the laser polarization axis, comes from autoionization of the $^1\Sigma_u^+ Q_1$ doubly excited states [14] [red curves in Fig. 1(d)]. Direct ionization to the $2p\pi_u$ continuum leads to fragments centered at 5 eV and peaked at 90°, but was kept very small by tuning the XUV spectrum. Multiple dynamical pathways contribute at higher kinetic energies (7–8 eV), of which the dominant ones are direct ionization to the $2p\sigma_u$ continuum (for molecules aligned parallel to the laser polarization) and excitation of the Q_2 doubly excited states [blue curves in Fig. 1(d)] (for molecules aligned perpendicular to the polarization axis). Accordingly, experiments with a lower XUV high energy cutoff showed a disappearance of the high energy (> 6 eV) channel, while retaining the lower energy (2–6 eV) channel due to autoionization of the $^1\Sigma_u^+ Q_1$ states.

In the presence of the IR field the spectra undergo significant changes, as can been seen in Figs. 1(a) and 1(b), which show kinetic energy spectra for parallel and perpendicular molecular alignment as red dashed lines. These curves were obtained by averaging the XUV-IR time delay over one full IR cycle. Figure 1(e) shows a corresponding momentum map. A bond-softening contribution appears prominently at low kinetic energies with an angular distribution that is peaked along the laser polarization axis [13,15]. At high kinetic energies ($E_k \approx 7$ eV) a significant enhancement is observed at all angles, in agreement with our previous observations [6]. This contribution will be the main topic of this Letter.

In Figs. 2(a) and 2(b) the kinetic energy spectra for fragments ejected parallel and perpendicular to the laser polarization are shown as a function of the XUV-IR time delay. A strong delay dependence is observed, with different parts of the spectrum oscillating with a period that is half the period of the IR laser. In Figs. 2(c) and 2(d) the ion yields from selected ionization channels are plotted as a function of delay. We note that the oscillations at high energy at 0° and 90° are out of phase. In addition, in Fig. 2(c) (parallel alignment) the oscillations at 3 and 7 eV are also out of phase.

We have performed calculations solving the time-dependent Schrödinger equation for a deuterium molecule interacting with an APT and IR field by using a close-coupling method [6,16]. In these calculations all electronic and vibrational degrees of freedom were taken into account. Current computational capabilities only allow us to

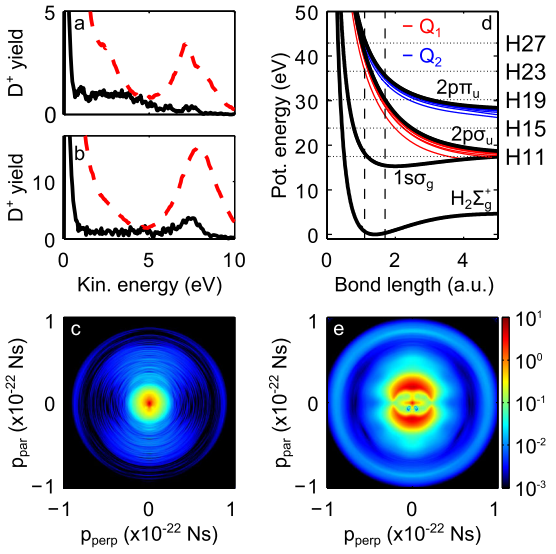

FIG. 1 (color online). Fragment kinetic energy spectra from dissociative ionization of D_2 at 0° (a) and at 90° (b) $\pm 20°$ by the APT only (black solid lines) and by the APT + IR (cycle averaged) at temporal overlap (red dashed lines). Corresponding momentum maps for the APT (c) and the APT + IR (e). In (d) a potential energy diagram is given indicating the relevant neutral (red and blue lines) and ionic (black lines) states. The Franck-Condon region is indicated by vertical dashed lines, and the position of a selection of harmonic orders present in the experiment are marked with horizontal dotted lines.

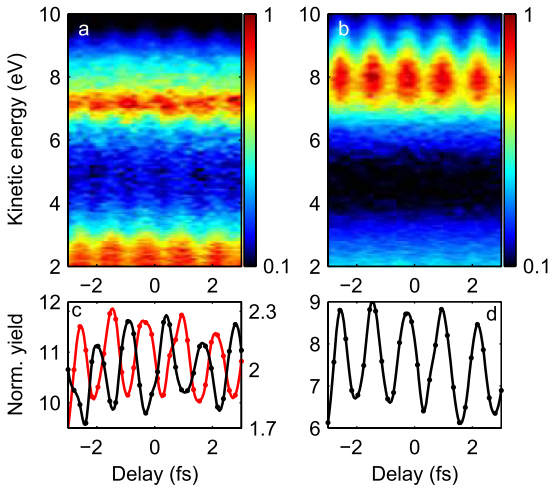

FIG. 2 (color online). Time-dependent fragment kinetic energy spectrum as a function of delay τ between the APT and the IR pulse for fragments ejected at 0° (a) and at 90° (b) $\pm 20°$. In (c) and (d) ion yields as a function of delay are plotted for parallel and perpendicular fragments where the signal is normalized to the yield by the APT only of that particular channel. In (c) the black [gray (red)] curve is for fragments centered at 7 [3] eV and in (d) fragments around 8 eV are shown.

consider the case where the molecule is aligned parallel to the laser polarization. Moreover, the pulse durations and intensities that can be explored are subject to restrictions. Therefore, in all the calculations presented here, an IR field with a sine squared envelope of 7.8 fs duration (2.8 fs FWHM), a central wavelength of 780 nm, and an intensity of 3×10^{12} W/cm^2 was combined with an APT consisting of 4 pulses, built from H13–H25.

In Fig. 3(a) the calculated fragment ion spectrum resulting from the interaction with the APT only is shown (black curve). This ion spectrum is dominated by the channels discussed before: direct ionization to the $1s\sigma_g$ continuum, autoionization of the $^1\Sigma_u^+ Q_1$ states to the $1s\sigma_g$ continuum, and direct ionization to the $2p\sigma_u$ continuum. In Fig. 3(b) the fragment ion yield as a function of kinetic energy and delay in the two-color XUV + IR field is given. The numerical results reproduce the experimentally observed yield oscillations at both high and low kinetic energies and a significant enhancement [red dashed line in Fig. 3(a)], although less pronounced than in the experiment due to the lower intensity used in the calculations.

The results reported here are reminiscent of earlier work, where oscillations in the He^+ yield were observed as a function of the APT-IR delay [17]. The oscillations were attributed to interferences between consecutive pulses in the APT and involved the excitation of Rydberg states. In contrast, our calculations show that yield oscillations occur both for an APT and for isolated attosecond pulses that remain present when the neutral Q_1 states are removed from the calculation. This shows that the origin of the oscillations in the current experiment is different. Our calculations suggest that the high energy fragments result from direct ionization to the $2p\sigma_u$ continuum, while the low energy fragments come from autoionization of the $^1\Sigma_u^+ Q_1$ states.

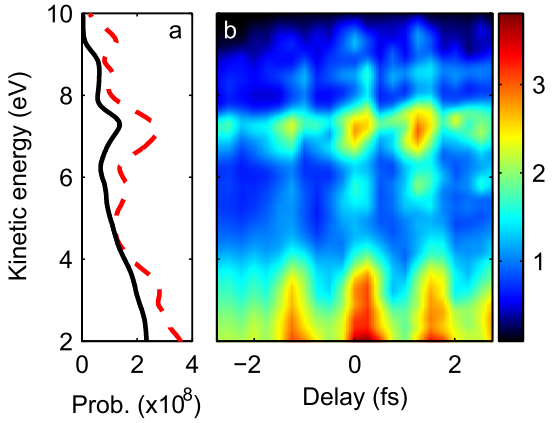

FIG. 3 (color online). Results of the close-coupling calculations for dissociative ionization of D_2 by a 4-pulse APT and a 2.8 fs FWHM 780 nm field with a peak intensity of 3×10^{12} W/cm^2. (a) Fragment kinetic energy spectra from the APT only (black solid line) and the APT + IR at $\tau = 0$ (red dashed line). (b) Fragment kinetic energy spectrum as a function of delay between the two pulses.

In order to arrive at a mechanistic interpretation of the observations at high fragment kinetic energies, it is instructive to explore a simpler model, using a fixed nuclei approximation (FNA). The wave function in this model is described in terms of a limited number of electronic states, including those that are relevant for the production of the high energy fragments:

$$\Psi(t) = c_0(t)\psi_0 + \sum_l \int d\epsilon c_{g,\epsilon l}(t)\psi_{g,\epsilon l} + \sum_l \int d\epsilon c_{u,\epsilon l}(t)\psi_{u,\epsilon l}, \quad (1)$$

where ψ_0 represents the ground state of the neutral molecule and $\psi_{g,\epsilon l}$ and $\psi_{u,\epsilon l}$ are the continuum wave functions of the molecular ion in the $1s\sigma_g$ and $2p\sigma_u$ states, respectively, plus one electron in the continuum with a partial wave l and energy ϵ. Continuum states with ungerade total symmetry Σ_u (ion + electron) are coupled with the ground state and with continuum states with gerade total symmetry Σ_g. The ground state is only coupled to Σ_g continuum states via the Σ_u states. The center of mass of the nuclear wave packet is shifted +0.3 a.u. with respect to the center of the Franck-Condon region (1.4 a.u.), since at an internuclear distance of 1.4. a.u. the energy gap between the ground state and the $2p\sigma_u$ continuum lies beyond the most intense part of the XUV spectrum (centered at H19).

In Fig. 4(a) the simulated total ionization probability to the $2p\sigma_u$ continuum, which correlates with the formation of high energy fragments, is plotted as a function of the delay between the APT and the IR for three different implementations of the FNA [see Fig. 4(b)]. In the first FNA calculation (blue dashed curve) only the $2p\sigma_u$ continuum is included and the couplings between states within the continuum are turned on, represented by the vertical red arrows in the darker (green) marked area in Fig. 4(b). These couplings result in the appearance of sidebands in the photoelectron spectrum in between the photoelectron peaks that result from direct ionization by the odd harmonics in the APT. The intensity of these sidebands oscillates with the XUV-IR delay as in RABBITT experiments [1], but this does not lead to an oscillation in the yield of the $2p\sigma_u$ state. A simulation including the coupling between the $1s\sigma_g$ and the $2p\sigma_u$ continua but without the couplings within the individual continua results in large oscillations of the ionization probability (solid red line). In Fig. 4(b) these couplings are illustrated by the diagonal red arrows. This situation again shows similarities to a RABBITT experiment; however, the odd harmonics primarily access the $1s\sigma_g$ continuum and the sideband appears in the $2p\sigma_u$ continuum. Absorption and emission of one IR photon from the direct photoelectron lines in the $1s\sigma_g$ continuum contribute to the sideband. These two pathways interfere constructively or destructively depending on the relative phase of the IR field and the XUV pulses. Correspondingly, the total ionization oscillates as a function of the delay with

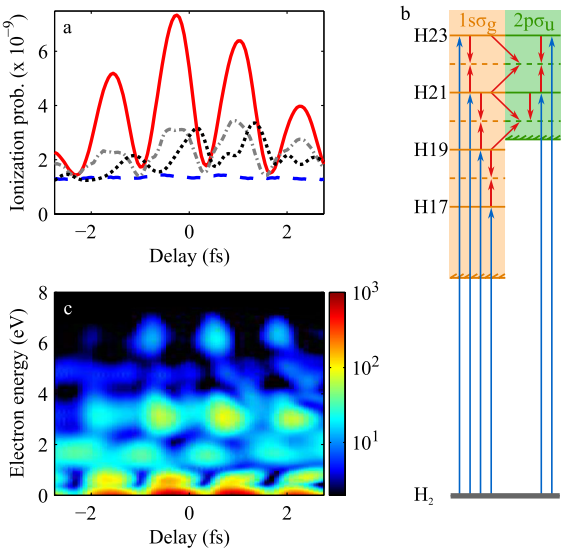

FIG. 4 (color online). (a) Calculated probability of ionization to the $2p\sigma_u$ continuum at an IR intensity of 3×10^{12} W/cm^2 in the FNA approximation. See text for a description of the individual curves. (b) Schematic illustration of APT + IR ionization to the $1s\sigma_g$ [lighter (orange) region] and $2p\sigma_u$ continuum [darker (green) region]. Long vertical blue arrows represent ionization by the odd harmonic orders of the APT, short red vertical arrows represent IR-induced couplings within the continua, and red diagonal arrows represent the coupling between the continua. (c) Calculated delay dependence of the photoelectron spectrum belonging to the solid red line in (a).

a period of half an optical IR cycle. This interpretation is further supported by the calculated photoelectron spectrum corresponding to ionization to the $2p\sigma_u$ continuum as a function of delay [see Fig. 4(c)]. The picture is modified when the couplings within the continua are turned on as well (gray dash-dotted line). The yield oscillations in this result are close to the result of the close-coupling calculation (black line), although they show a phase difference, which is attributed to the simplicity of the FNA model, where only one fixed internuclear distance is considered. We note that because the ionization cross section of the $1s\sigma_g$ continuum is much larger than that of the $2p\sigma_u$ continuum, even a small IR-induced coupling can significantly affect the ionization to the $2p\sigma_u$ continuum while leaving ionization to the $1s\sigma_g$ continuum effectively unaffected.

The frequency-domain interpretation given above can be complemented by a description in the time domain. The XUV-IR delays where a destructive interference is observed correspond to delays where the attosecond pulses in the APT are positioned at zero crossings of the IR field, whereas delays where a constructive interference is observed correspond to delays where the attosecond pulses in the APT are positioned at (negative or positive) maxima of the IR electric field. In the presence of a strong electric field the eigenstates of the Hamiltonian are no longer the $1s\sigma_g$ and $2p\sigma_u$ states, but are linear combinations of these states [18], where the electron distribution is no longer symmetric but the molecule is polarized. Hence, an alternative way to view the experimental results is that the XUV ionization favors the production of the $2p\sigma_u$ state when—under the influence of the IR field—this state is mixed with the $1s\sigma_g$ state, with an accompanying localization of the electron within the molecule. As such, our experiment lends support to the notion that in attosecond ionization experiments changes in the charge distribution on attosecond time scales can be revealed, which is a core objective for future work.

This work is part of the research program of the "Stichting voor Fundamenteel Onderzoek der Materie (FOM)," which is financially supported by the "Nederlandse organisatie voor Wetenschappelijk Onderzoek (NWO)." We thank Mare Nostrum BSC and CCC-UAM for allocation of computer time. Work partially supported by the MICINN Projects No. FIS2010-15127, No. ACI2008-0777, and No. CSD 2007-00010, MC-ITN ATTOFEL, and the European COST Action CM0702. P. J. acknowledges support from the Swedish Research Council.

[1] P. M. Paul *et al.*, Science **292**, 1689 (2001).
[2] M. Hentschel *et al.*, Nature (London) **414**, 509 (2001).
[3] M. Drescher *et al.*, Nature (London) **419**, 803 (2002).
[4] M. Uiberacker *et al.*, Nature (London) **446**, 627 (2007).
[5] A. L. Cavalieri *et al.*, Nature (London) **449**, 1029 (2007).
[6] G. Sansone *et al.*, Nature (London) **465**, 763 (2010).
[7] F. Remacle and R. D. Levine, Proc. Natl. Acad. Sci. U.S.A. **103**, 6793 (2006).
[8] A. I. Kuleff and L. S. Cederbaum, Chem. Phys. **338**, 320 (2007).
[9] M. F. Kling *et al.*, Science **312**, 246 (2006).
[10] K. P. Singh *et al.*, Phys. Rev. Lett. **104**, 023001 (2010).
[11] A. T. J. B. Eppink and D. H. Parker, Rev. Sci. Instrum. **68**, 3477 (1997).
[12] O. Ghafur, W. Siu, P. Johnsson, M. F. Kling, M. Drescher, and M. J. J. Vrakking, Rev. Sci. Instrum. **80**, 033110 (2009).
[13] F. Kelkensberg *et al.*, Phys. Rev. Lett. **103**, 123005 (2009).
[14] K. Ito, R. I. Hall, and M. Ukai, J. Chem. Phys. **104**, 8449 (1996).
[15] P. H. Bucksbaum, A. Zavriyev, H. G. Muller, and D. W. Schumacher, Phys. Rev. Lett. **64**, 1883 (1990).
[16] J. L. Sanz-Vicario, H. Bachau, and F. Martin, Phys. Rev. A **73**, 033410 (2006).
[17] P. Johnsson, J. Mauritsson, T. Remetter, A. L'Huillier, and K. J. J. Schafer, Phys. Rev. Lett. **99**, 233001 (2007).
[18] P. Dietrich, M. Y. Ivanov, F. A. Ilkov, and P. B. Corkum, Phys. Rev. Lett. **77**, 4150 (1996).